Arch. Metall. Mater. **66** (2021), 3, 759-763

DOI: 10.24425/amm.2021.136376

GWANGHUN KIM[1], JUNHYUB JEON[1], NAMHYUK SEO[1], SEUNGGYU CHOI[1], MIN-SUK OH[1], SEUNG BAE SON[1], SEOK-JAE LEE[1*]

EFFECT OF SINTERING HOLDING TIME AND COOLING RATE ON THE AUSTENITE STABILITY AND MECHANICAL PROPERTIES OF NANOCRYSTALLINE FeCrC ALLOY

The effects of the sintering holding time and cooling rate on the microstructure and mechanical properties of nanocrystalline Fe-Cr-C alloy were investigated. Nanocrystalline Fe-1.5Cr-1C (wt.%) alloy was fabricated by mechanical alloying and spark plasma sintering. Different process conditions were applied to fabricate the sintered samples. The phase fraction and grain size were measured using X-ray powder diffraction and confirmed by electron backscatter diffraction. The stability and volume fraction of the austenite phase, which could affect the mechanical properties of the Fe-based alloy, were calculated using an empirical equation. The sample names consist of a number and a letter, which correspond to the holding time and cooling method, respectively. For the 0A, 0W, 10A, and 10W samples, the volume fraction was measured at 5.56, 44.95, 6.15, and 61.44 vol.%. To evaluate the mechanical properties, the hardness of 0A, 0W, 10A, and 10W samples were measured as 44.6, 63.1, 42.5, and 53.8 HRC. These results show that there is a difference in carbon diffusion and solubility depending on the sintering holding time and cooling rate.

Keywords: Fe-Cr-C alloy, Sintering holding time, Cooling rate, Austenite stability, Nanocrystalline

1. Introduction

High-carbon chromium steel is widely used as bearing steel in various parts found in industrial machinery, automobiles, and aircraft. Recent industrial developments demand that such parts maintain high functionality and high performance even under harsh operating conditions. The bearing steel must therefore have excellent mechanical properties, such as high strength, wear resistance, and fatigue life of bearing steel. Retained austenite is representative of the factors affecting the properties of bearing steel [1-3].

The retained austenite is transformed to strain-induced martensite during plastic deformation, improving the ductility and tensile strength of the steel [4-7]. Therefore, controlling the stability and the volume fraction of austenite at room temperature is an important factor in determining the mechanical properties of the alloy.

Austenite stability is affected by the chemical composition [8,9] and grain size [10,11]. As the amount of the austenite-stabilizing elements such as C and Mn increased, and the austenite stability increased. In particular, the thermodynamic stability of the austenite increases the martensite start (Ms) temperature during cooling is lowered when C is dissolved in the austenite lattice. Grain refinement is also effective in increasing the stability of austenite. Lee et al. [12] reported that a high volume fraction of austenite was obtained by reducing the grain size to 300 nm in ultra-fine-grained TRIP steel containing 6 wt.% Mn.

Powder metallurgy uses conventional manufacturing processes that overcome the limitations of grain refinement. Mechanical alloying (MA) is performed by mixing powdered of metals and ceramics using a high-energy ball mill, and it is easy to manufacture nanostructured alloys and compounds [13]. Among sintering methods, spark plasma sintering (SPS) has been reported for nanocrystalline structures, ceramic materials, and iron-based materials. SPS suppresses grain growth by pressurizing the mold containing the powder and heating it using a pulse current to sinter it in a short time [14,15]. However, although many studies have been conducted on bearing steel manufactured by conventional processes, few studies focused on the use of powder metallurgy in the construction of bearing steel.

To address this deficit, we used powder metallurgy to control the sintering holding time and cooling rate to investigate the

[1] JEONBUK NATIONAL UNIVERSITY, DIVISION OF ADVANCED MATERIALS ENGINEERING, 567 BAEKJE-DAERO, DEOKJIN-GU, JEONJU, 54896, REPUBLIC OF KOREA

* Corresponding author: seokjaelee@jbnu.ac.kr

effect of these parameters on the stability of the austenite and the mechanical properties of the Fe-Cr-C alloy. Differences in the diffusion and solubility of carbon under different sintering conditions and their effects on the austenite stability and mechanical properties of the Fe-Cr-C alloy were investigated.

2. Experimental procedure

Fe powder (Alfa Aesar, Korea) of 99% purity and an average particle size (APS) of <74 μm, Cr powder (Alfa Aesar, Korea) of 99% purity and APS of <140 μm, graphite powder (Alfa Aesar, Korea) of 99% purity and APS of 7-11 μm were mixed by a high-energy ball mill (a Pulverisette-6 planetary mill) at 250 rpm for 24 hour under a pure Ar atmosphere to fabricate nanocrystalline Fe-1.5Cr-1C (wt.%) alloy powder. The ball milling time was 24 cycles and one cycle includes 1 hour of milling time and 30 minutes of rest. Stainless containers and tungsten carbide balls with a diameter of 10 mm were used, and the ratio of balls to powder was set at 30:1. 1.0 wt.% stearic acid was added as a process control agent to adjust the balance of cold welding and fracturing, and the BN lubricant was sprayed into a graphite mold to prevent powder welding during sintering. The milled alloy powder was placed into a cylindrical graphite mold with an outer diameter of 35 mm, an inner diameter of 10 mm, and a height of 40 mm, and sintered using SPS at a rate of 1000°C/min to 1000°C under a high vacuum of 150 mTorr and a uniaxial pressure of 80 MPa. The sintering process conditions are shown in Table 1.

As shown in Table 1, the samples names consist of a number and a letter, which correspond to the holding time and cooling method, respectively (e.g., "0A" denotes an air cooled sample with no holding time). The relative density of the sintered alloy was determined using the Archimedes method. The structural properties of the powder, including the grain size, were analyzed using Williamson-Hall analysis. Phase analysis was performed using X-ray diffraction (XRD) at 40 kV and 30 mA with a Cu Kα source (Shimadzu, XRD-6100). The sample was analyzed in the 2θ range of 30-100° with a scan speed of 2°/min. The volume fraction of the austenite phase was measured using the intensity of the XRD and electron backscatter diffraction (EBSD) diffraction peaks. The lattice parameter of austenite was calculated from the XRD results using the Nelson-Riley equation. The mechanical properties of the sintered alloys were measured using a Rockwell hardness tester (SSAUL BESTECH, BSETROC-300N).

TABLE 1

Sintering process conditions of Fe-1.5Cr-1C alloy samples

Name	Temperature (°C)	Holding time (min)	Cooling method
0A	1000	0	air cooling
0W	1000	0	water quenching
10A	1000	10	air cooling
10W	1000	10	water quenching

3. Results and discussion

Fig. 1 shows the XRD patterns of the raw powders and the Fe-Cr-C alloy powder obtained using MA with a high-energy ball mill. Only a single α-Fe peak was observed in the diffraction pattern of the alloy powder, which confirms that the added elements were mechanically alloyed in the Fe base. The crystallite size of the powder was calculated using the Williamson–Hall equation using the full width at half maximum (FWHM) and Bragg angles of the XRD peak [16]:

$$\beta_r \cos\theta = \frac{k \cdot \lambda}{D} + \eta \sin\theta \quad (1)$$

where β_γ is the FWHM of the milled alloy powder XRD peak, θ is the Bragg angle, λ is the wavelength of the Cu K_α source, k is a constant, D is the crystallite size, and η is the lattice strain. The crystallite size of the alloy powder is approximately 10 nm.

An Fe-Cr-C alloy powder samples were manufactured by MA and sintered using SPS. The sintering conditions were varied by adjusting the sintering holding time and cooling method (Table 1). The relative density was obtained from the measured density and theoretical density was calculated using the mixing ratio of the sintered alloy. The relative densities of 0A, 0W, 10A, and 10W were 98.73, 97.90, 99.89, and 99.80 %, respectively, and the density of the samples corresponded to the theoretical density due to densification during SPS.

Fig. 2 shows the XRD patterns of the sintered samples. The phase and peak intensities changed depending on the sintering process conditions. The diffraction patterns of the 0A and 10A samples showed an α-Fe peak and some cementite peaks, while those of the 0W and 10W samples showed α-Fe and γ-Fe peaks. The cooling time of the water-quenched samples was too short for carbon diffusion to occur, so cementite was not detected, and carbon was present in the austenite lattice.

Fig. 3 shows the austenite phase fraction of the sintered alloy, as measured by XRD and EBSD. The austenite phase fraction was calculated by applying the Averbach-Cohen equation to the XRD results, and the volume fractions of 0A, 0W, 10A, and 10W were measured as 5.56, 44.95, 6.15, and 61.44 vol.%, respectively [17]. The austenite phase fraction obtained by EBSD analysis was similar to that obtained by XRD. In general Fe-based alloys, austenite is only thermodynamically stable at high temperatures, so the phase fractions found at room temperature are usually very small. However, when austenite-stabilizing elements such as C and Mn are added, the austenite stability increases, and the austenite fraction can be stabilized at room temperature. Previous studies have shown that intercritical annealing treatment of Fe-Mn-C alloy at 650°C for up to 144 h can increase the austenite fraction found at room temperature to 45% [18]. However, sintered Fe-Mn-C alloys of the same composition produced by powder metallurgy have been found to contain high austenite fractions of up to 97% [19]. It was determined that the grain refinement also affected the austenite stability Because the austenite fraction in samples with better grain refinement reached 61% in this study. Fig. 3(a) shows the

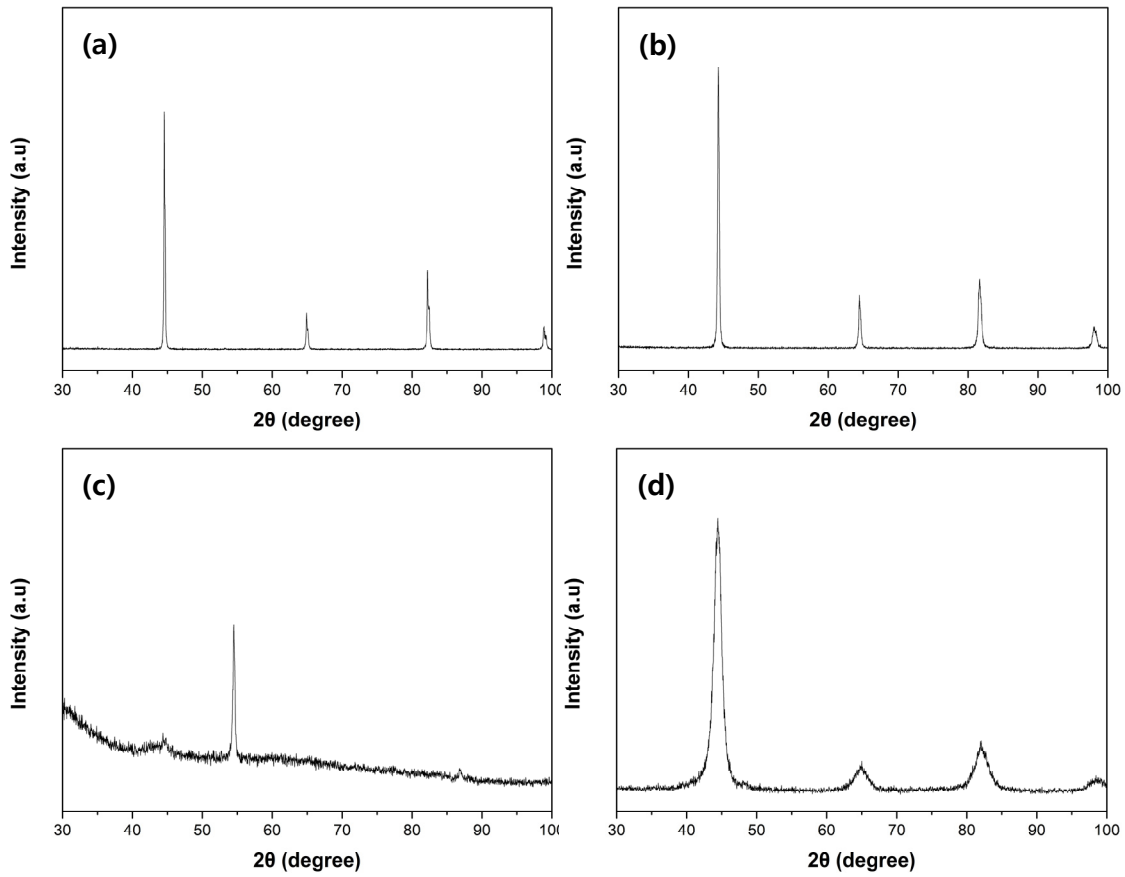

Fig. 1. XRD patterns of the raw and milled powders: (a) Fe powder, (b) Cr powder, (c) Graphite powder, and (d) milled Fe-1.5Cr-1C powder

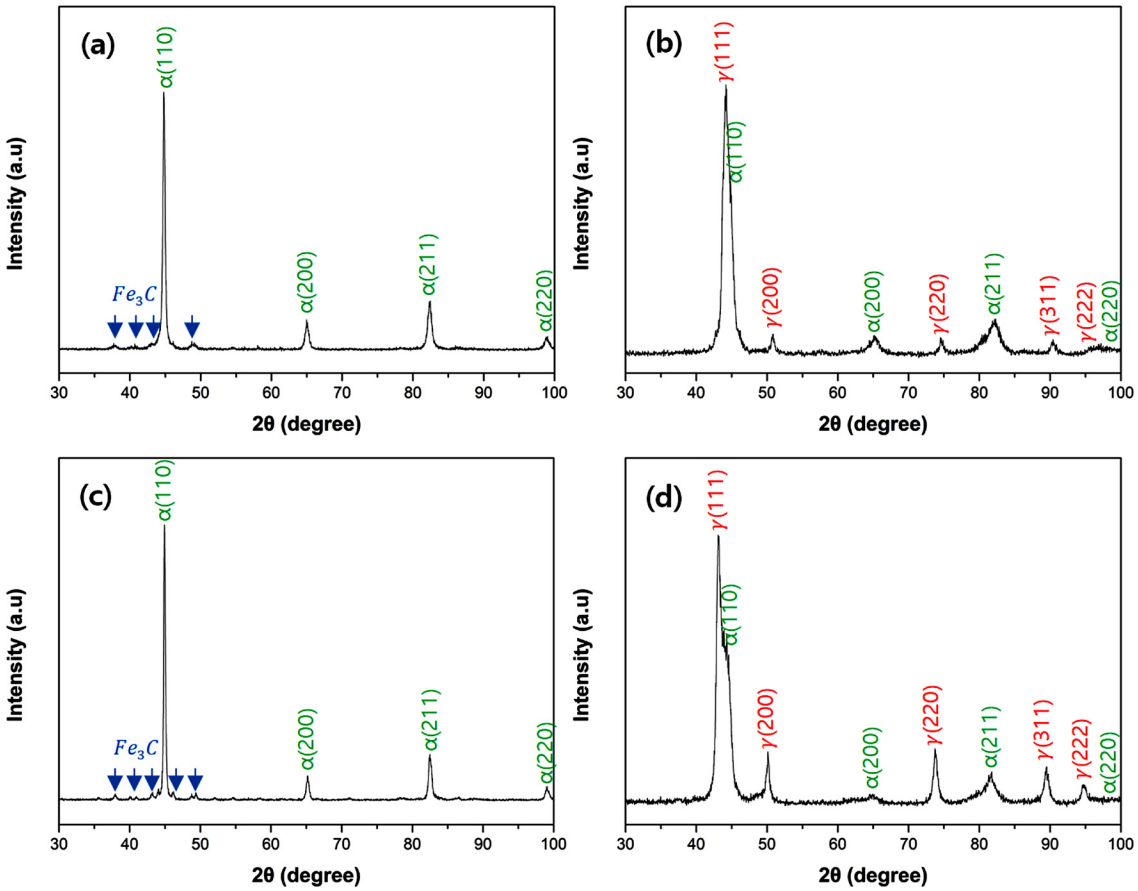

Fig. 2. XRD patterns of the sintered Fe-1.5Cr-1C samples: (a) 0A, (b) 0W, (c) 10A, and (d) 10W

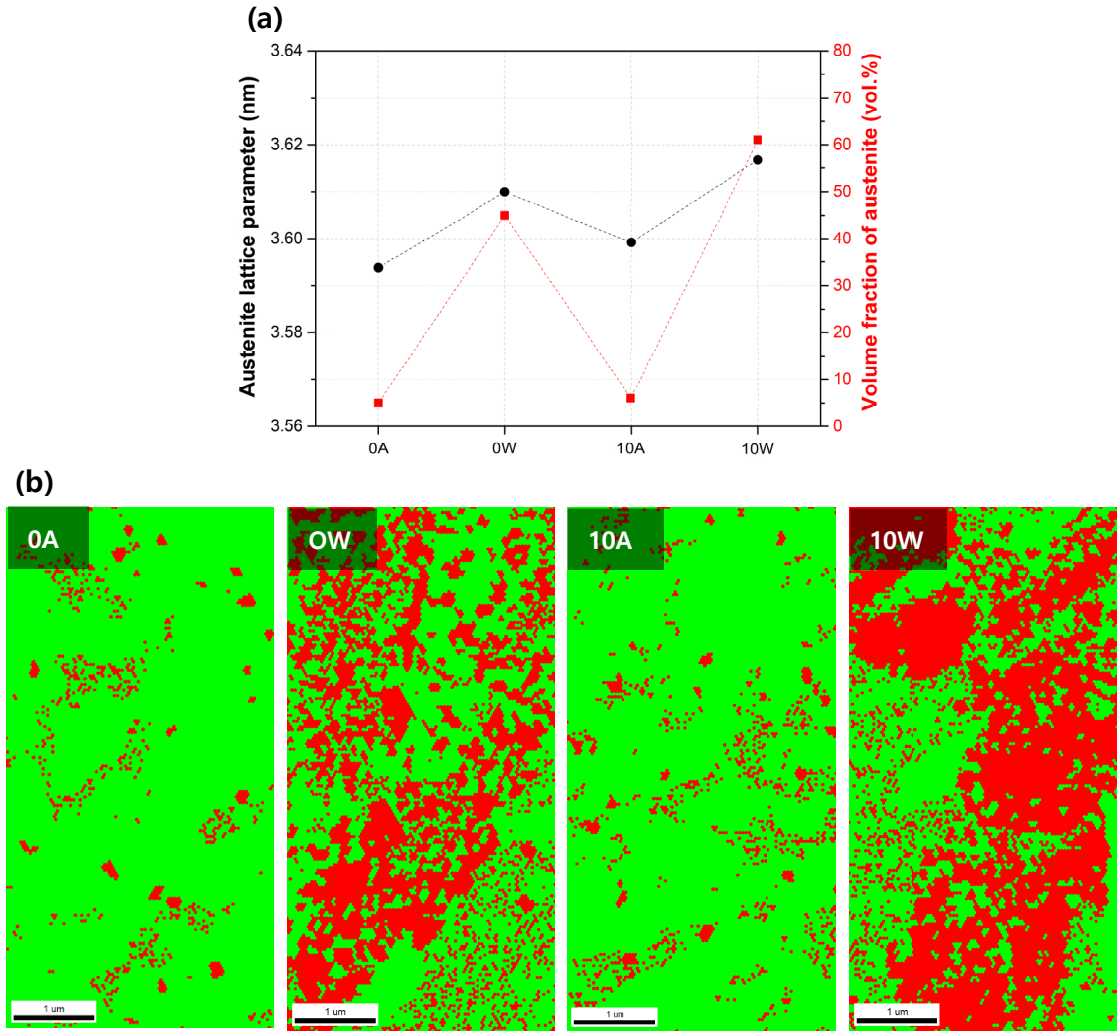

Fig. 3. Phase analysis results of sintered samples by (a) XRD and (b) EBSD (green : ferrite, red : austenite)

relationship between the austenite fraction and the austenite lattice parameter of the sintered alloy. The austenite lattice parameter of the sintered alloy was calculated from the XRD results using the Nelson-Riley equation [20]. The austenite fraction of the sintered alloy increases in proportion to the lattice constant. The water-quenched samples showed a high lattice parameter compared to the air-cooled samples with the same sintering holding time. Water-quenched samples were cooled too quickly for carbon diffusion to occur, so cementite was not detected, and carbon was present in the austenite lattice. Accordingly, the austenite lattice parameter differed based on the cooling rate. Samples with increased sintering holding times at the same cooling rate showed a high lattice parameter. This is because carbon diffuses into the austenite lattice during the sintering holding time and the amount of carbon in the lattice increases, we therefore concluded that the difference in austenite lattice parameter is due to the sintering holding time. The austenite fraction of the sintered alloy increased as the carbon content in the austenite lattice increased owing to changes in the sintering holding time and cooling rate.

Fig. 4 shows the relationship between the dislocation density and the hardness of the sintered alloy. The value of the dislocation density was calculated using the crystallite size and the micro-strain obtained from the Williamson-Hall equation based on the XRD results. Dislocation density can be calculated by an equation given below [21]:

$$\rho = \frac{3\sqrt{2\pi}(\varepsilon^2)^{1/2}}{Db} \tag{2}$$

where p is dislocation density, ε is micro-strain, D is crystallite size, b is burgers vector. The dislocation densities of the 0A, 0W, 10A, and 10W samples were calculated to be 1.20, 7.36, 1.02, 4.67 ($\times 10^{12}$ m^{-2}), and the hardness was measured as 44.6, 63.1, 42.5, and 53.8. Samples with an increased sintering holding time at the same cooling rate exhibited low hardness. It was determined that grain growth occurred during the sintering holding time owing to the Hall-Petch equation, resulting in a decrease in hardness. The water-quenched samples showed higher hardness values than the air-cooled samples, for a given sintering holding time. One previous study reported that the sintered samples manufactured by water-quenching duplex stainless steel made by powder metallurgy had a martensite phase and thus had better hardness than the furnace-cooled sample [22]. The water-

quenched samples in our study were similarly judged to have high hardness owing to the formation of the martensite phase. The high dislocation density of the samples can be explained by the fast cooling rate.

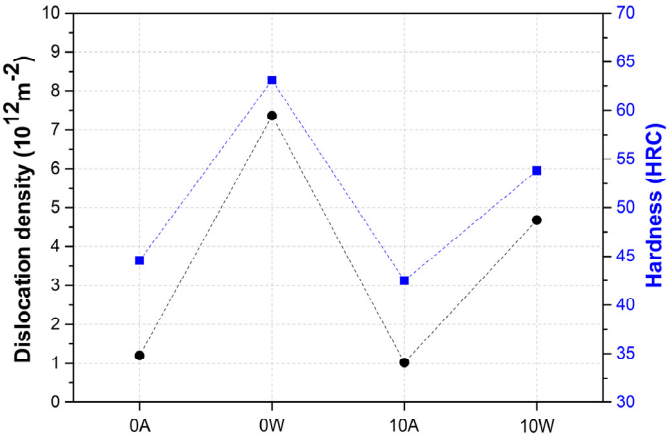

Fig. 4. Relationship between dislocation density and hardness

4. Conclusions

Nanocrystalline Fe-1.5Cr-1C (wt%) alloy was fabricated using a high-energy ball mill and SPS. Sintered alloys were fabricated by controlling the sintering holding time and cooling rate. The longer the sintering holding time, the higher the carbon content of the austenite lattice, resulting in higher austenite lattice parameter and austenite phase fractions. Water-quenching of the samples prevented the formation of cementite due to the short cooling time, and carbon was dissolved in the austenite lattice, resulting in a high austenite fraction. The hardness according to the sintering process conditions increased in the order of 0W, 10W, 0A, and 10A. This result was due to a number of complex influences such as grain size, phase fraction, and dislocation density, which are determined by the sintering holding time and cooling rate. These results confirm that the difference in carbon diffusion and solubility were due to changes in the sintering holding time and cooling rate, thereby affecting the mechanical properties.

Acknowledgments

This work was supported by a Korea Institute for Advancement of Technology grant, funded by the Korea Government (MOTIE) (P0002019), as part of the Competency Development Program for Industry Specialists.

REFERENCES

[1] E. Yajima, T. Miyazaki, T. Sugiyama, H. Terajima, Trans. JIM **15**, 173 (1974).
[2] E.C. Santos, K. Kida, T. Honda, J. Rozwadowska, K. Houri, Adv. Mater. Res. **217**, 982 (2011).
[3] I. Yoshida, K. Yamamoto, K. Domura, K. Mizobe, K. Kida, Mater. Sci. Forum **867**, 55 (2016).
[4] O. Grassel, L. Kruger, G. Frommeyer, L.W. Meyer, Int. J. Plast. **16**, 1391 (2000).
[5] G. Frommeyer, U. Brux, P. Neumann, ISIJ Int. **43**, 438 (2003).
[6] D.S. Park, S.J. Oh, I.J. Shon, S.J. Lee, Arch. Metall. Mater. **63**, 1479 (2018).
[7] S.G. Choi, J.H. Jeon, N.H. Seo, Y.H. Moon, I.J. Shon, S.J. Lee, Arch. Metall. Mater. **65**, 1001 (2020).
[8] S.J. Lee, S. Lee, B.C. De Cooman, Scr. Mater. **64**, 649 (2011).
[9] Y. Sakuma, O. Matsumura, H. Takechi, Met. Trans. A **22**, 489 (1991).
[10] Y. Matsuoka, T. Iwasaki, N. Nakada, T. Tsuchiyama, S. Takaki, ISIJ Int. **53**, 1224 (2013).
[11] K. Sugimoto, M. Misu, M. Kobayashi, H. Shirasawa, ISIJ Int. **33**, 775 (1993).
[12] S.J. Lee, S. Lee, B.C. De Cooman, Int. J. Mater. Res. **104**, 423 (2013).
[13] J.S. Benjamin, T.E. Volin, Met. Trans. **5**, 1929 (1974).
[14] S.I. Cha, S.H. Hong, B.K. Kim, Mater. Sci. Eng. A **351**, 31 (2003).
[15] H.W. Zhang, R. Gopalan, T. Mukai, K. Hono, Scr. Mater. **53**, 863 (2005).
[16] G.K. Williamson, W.H. Hall, Acta Metall. **1**, 22 (1953).
[17] B.L. Averbach, M. Cohen, Trans. AIME **176**, 401 (1948).
[18] H. Luo, J. Shi, C. Wang, W. Cao, X. Sun, H. Dong, Acta Mater. **59**, 4002 (2011).
[19] S.J. Oh, J.H. Jeon, I.J. Shon, S.J. Lee, J. Korean Powder Metall. Inst. **26**, 389 (2019).
[20] I. Seki, K. Nagata, ISIJ Int. **45**, 1789 (2005).
[21] G. Dini, R. Ueji, A. Najafizadeh, S.M. Monir-Vaghefi, Mater. Sci. Eng. A **527**, 2759 (2010).
[22] F. Martin, C. Garcia, Y. Blanco, M.L. Rodriguez-Mendez, Mater. Sci. Eng. A **642**, 360 (2015).